Microporous and Mesoporous Materials 163 (2012) 34–41

Contents lists available at SciVerse ScienceDirect

Microporous and Mesoporous Materials

journal homepage: www.elsevier.com/locate/micromeso

Phase behavior of mesoporous silicas templated by the amphiphilic diblock copolymer poly(ethylene-*b*-ethylene oxide)

Jheng-Guang Li, Wei-Chih Chen, Shiao-Wei Kuo *

Department of Materials and Optoelectronic Science, Center for Nanoscience and Nanotechnology, National Sun Yat-Sen University, Kaohsiung 804, Taiwan

ARTICLE INFO

Article history:
Received 17 April 2012
Received in revised form 10 June 2012
Accepted 11 June 2012
Available online 6 July 2012

Keywords:
Block copolymers
Evaporation-induced self-assembly
Mesoporous silica
Mesophase transition
Sol–gel process

ABSTRACT

In this study we used an amphiphilic diblock copolymer, poly(ethylene-*b*-ethylene oxide) (PE-*b*-PEO), as an organic template for the synthesis of mesoporous silica through evaporation-induced self-assembly (EISA). Using transmission electron microscopy (TEM), small-angle X-ray scattering (SAXS), and nitrogen adsorption/desorption isotherms, we investigated the effects of the tetraethyl orthosilicate (TEOS) and hydrochloric acid (HCl) contents on the EISA process. At a constant $HCl_{(aq)}$-to-PE-*b*-PEO ratio (0.12:1), we observed an interesting mesophase transition—from lamellae to distorted lamellae to cylinders mixed with spheres to spherical structures—upon increasing the TEOS-to-PE-*b*-PEO ratio. Meanwhile, at a constant TEOS-to-PE-*b*-PEO ratio (10:1), a mesophase transition from distorted lamellae to cylinders mixed with spheres to single spherical morphology occurred upon decreasing the $HCl_{(aq)}$-to-PE-*b*-PEO ratio. Because the TEOS-to-PE-*b*-PEO ratio changed the volume fraction of the microphase separation system and the $HCl_{(aq)}$-to-PE-*b*-PEO ratio affected the rate of hydrolysis of TEOS during the EISA process, we attribute the various mesophase phenomena to competition between thermodynamic and kinetic control, respectively. In addition, we also observed a metastable structure, so-called "buckled cylinders," in some of our systems.

1. Introduction

Although the number of publications relating to the synthesis of mesoporous materials such as M41S and SBA-n has been increasing steadily [1–16], our understanding of the mechanisms behind these procedures remains limited. At present, three kinds of mechanisms have been established for the fabrication of mesoporous nanostructures [17–19]: precipitation-based methods [20,21], true liquid crystal templating (TLCT) methods [22–24], and evaporation-induced self-assembly (EISA) methods [25–28]. Among them, the EISA method is particularly convenient because it can be applied in various non-aqueous synthesis [17,18], especially when using amphiphilic block copolymers as templates; nevertheless, only a few attempts have been made to understand this process. EISA can be considered a liquid crystal templating (LCT)-based method; after solvent evaporation, a hybrid liquid crystal (LC) phase is formed and high dilution discourages inorganic polymerization. Amphiphilic block copolymers lose their joint hydrophilic/hydrophobic properties when large amounts of weak-polarity solvents are present—because both their hydrophilic and hydrophobic segments interact with these solvents simultaneously, thereby inhibiting the self-assembly of the amphiphilic block copolymers. Upon further evaporation-induced crowding, these aggregates (including organic block copolymer and inorganic oligomer) interact to form mesophases, the structures of which are influenced by the possibility of equilibrium phase behavior occurring in the presence of the solvent(s) and surfactant.

The mechanism of formation of these mesophases can be divided into two parts: the creation of an organized texture and the formation of an inorganic network. In their cooperative assembly model, Huo et al. defined [29] the most relevant thermodynamic aspects of the formation of a hybrid mesophase (ΔG_{ms}) using the equation.

$$\Delta G_{ms} = \Delta G_{inter} + \Delta G_{inorg} + \Delta G_{org} + \Delta G_{sol}$$

where ΔG_{inter} is the free energy associated with the interaction between the inorganic species and the amphiphilic molecule micelles [adequate segregation of the hydrophilic and hydrophobic regions of the template (mainly ΔG_{org}) requires, in principle, $|\Delta G_{inorg}| < |G_{inter}|or|\Delta G_{org}|$ to permit the latter two terms to direct the formation of organized assemblies]; ΔG_{inorg} is the structural free energy for the inorganic frameworks; and ΔG_{sol} is the chemical potential associated with the species in the solution phase. For the surfactant-templated assembly of mesostructured silicates, ΔG_{sol} can be regarded as a constant in a normal water-soluble system. Therefore, establishing a well-defined templated hybrid is a matter of controlling the delicate thermodynamic and kinetic balance between multiple phenomena. From a kinetics point of view, the

* Corresponding author. Tel.: +886 7 5252000x4079; fax: +886 7 5254099.
E-mail address: kuosw@faculty.nsysu.edu.tw (S.-W. Kuo).

1387-1811/$ - see front matter © 2012 Elsevier Inc. All rights reserved.
http://dx.doi.org/10.1016/j.micromeso.2012.06.017

role of inorganic condensation is a race toward order; the formation of an organized hybrid mesostructure is the result of the balance between two competitive processes: (i) phase separation or organization of the template and (ii) inorganic polymerization. In a typical precipitation-based synthesis, the kinetic constants (k_i) of the various processes underlie the formation of an ordered mesophase; they should follow the order [29].

$$k_{inter} > k_{org} > k_{inorg}$$

To obtain highly ordered mesoporous nanostructures, the kinetic constant for interfacial assembly of the organic and inorganic species must be higher than those for both the self-assembly of organic species and the condensation of inorganic species.

Block copolymers (BCPs) are versatile templates for the creation of mesostructured and mesoporous materials [19,30–32]. Great advances in recent years [33–42] have made it possible to obtain highly controlled large-pore and highly stable mesostructured and mesoporous materials (silica, non-silica oxides, carbons), shaped as powders, films, monoliths, or aerosols. The hydrophilic-to-hydrophobic volume ratio is especially important when using nonionic surfactant templating systems to form a particular mesophase [43,44]. In addition, the weight fraction of inorganic species (e.g., tetraethyl orthosilicate (TEOS), silica) can also affect the mesophase after the EISA process because it increases the volume fraction of the hydrophilic domain.

Both thermodynamic and kinetic effects influence the morphologies of the mesophases of the self-assembled nanostructures formed during the EISA process. In this study, we used a commercial PE-*b*-PEO block copolymer (M_n = 1400; PE = 50 wt.%) as our model template to fabricate various mesoporous silica structures using the EISA strategy, varying the TEOS-to-PE-*b*-PEO or HCl-to-PE-*b*-PEO ratio to determine the effects of the TEOS content and rates of hydrolysis and condensation from thermodynamic and kinetic points of view. The self-assembly behavior of pure PE-*b*-

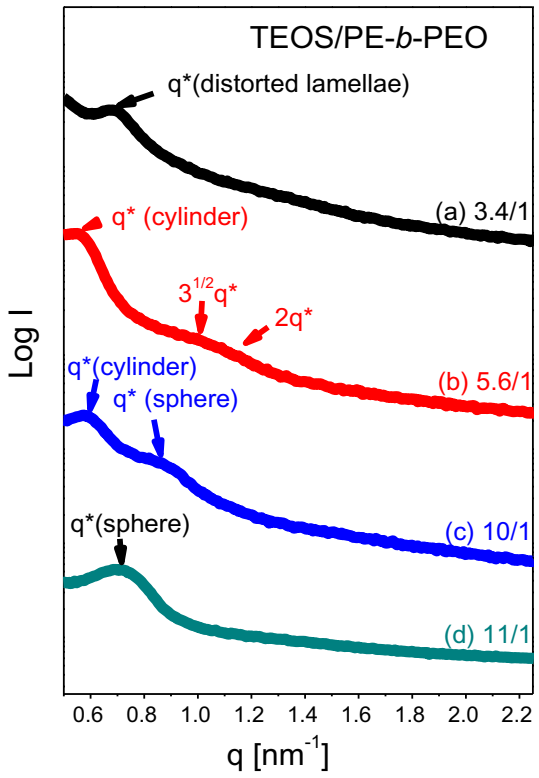

Fig. 1. SAXS patterns of mesoporous silica samples prepared at various TEOS-to-PE-*b*-PEO weight ratios.

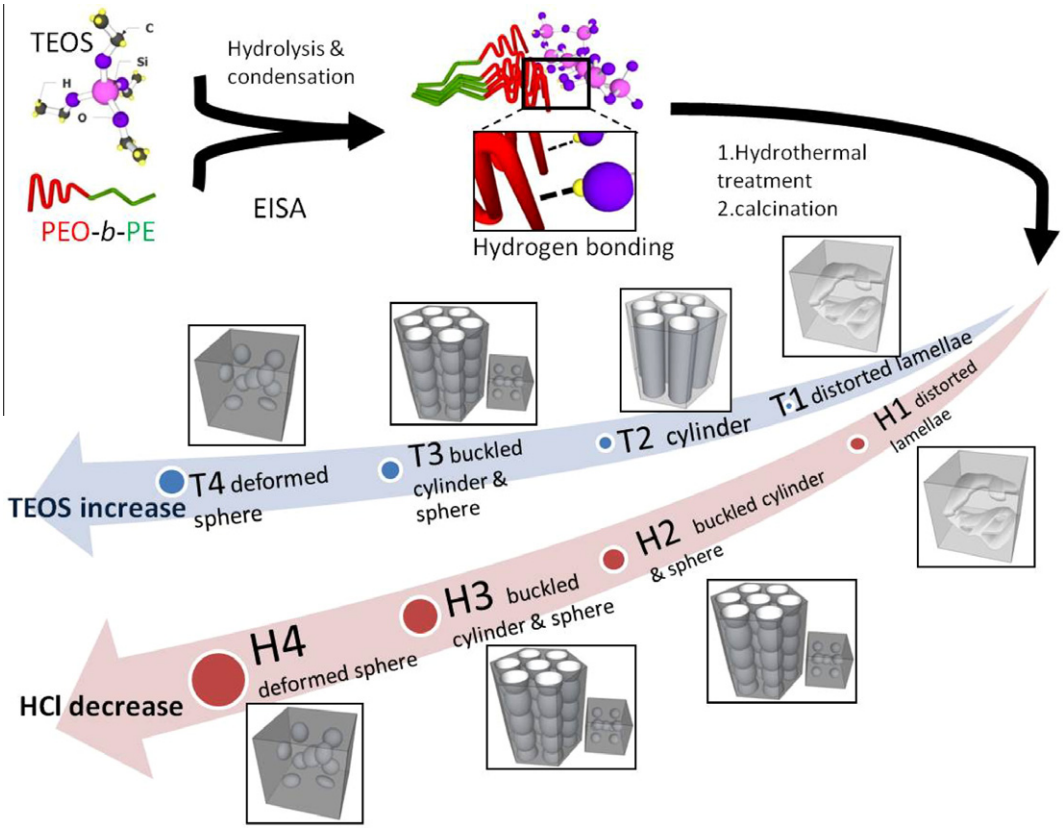

Scheme 1. Preparation of mesoporous silica samples under and morphology change with TEOS increase or HCl derease, respectively.

PEO diblock copolymer has studied in the previous work [46], however, the phase behaviors of mesoporous silica that templated by PE-*b*-PEO diblock copolymer is never discussed. Furthermore, mesoporous silicas would have excellent performances in various applications because the high surface area, stable structure and so on. Here, we used transmission electron microscopy (TEM), small-angle X-ray scattering (SAXS), and Brunauer–Emmett–Teller (BET) measurements to characterize the mesophase transformations occurring during the EISA process. Furthermore, we also observed the interesting structure that called buckled cylinder during the phase-transition, which is consistent with previous study by using different block copolymer system [45].

2. Experimental

2.1. Materials

All chemicals were used as received without purification. The PE-*b*-PEO diblock copolymer ($EO_{20}E_{29}$, 50 wt.% PEO; M_n = 1400) was purchased from Aldrich Chemical. TEOS (99%) and hydrochloric acid were obtained from SHOWA. EtOH (95%) and tetrahydrofuran (THF,>99%) were purchased form ECHO. De-ionized water was used in all experiments.

2.2. Synthesis of the mesoporous silica [39,42]

Mesoporous silica was prepared through an EISA strategy in THF, using the copolymer PE-*b*-PEO as a template and TEOS as the silica precursor (Scheme 1). In a typical synthesis, a TEOS-to-PE-*b*-PEO ratio of 3.4, 5.6, 10, or 11 was used at a constant HCl concentration (0.012 g of 0.1 M HCl/PE-b-PEO) or a HCl (0.1 M)-to-PE-*b*-PEO ratio of 0.06, 0.12, 0.16, or 0.8 was used at constant TEOS amount of 1.0 g, the TEOS and HCl with specific composition was added into a 5 g of THF solution of PE-b-PEO (2.0 wt.%, containing 0.10 g of copolymer), with stirring, which was continued for 30 min to form a homogeneous solution. The sample was poured into a Petri dishes and the THF was evaporated at room temperature for 48 h. The transparent film was collected and ground into a powder, which was then transferred to a PFA bottle containing 1.0 M HCl (30 mL) and hydrothermally treated at 100 °C for 3 days. The product was washed with water and EtOH, dried at room temperature, and calcined in air at 600 °C for 6 h to produce a white mesoporous silica. Both calcination processes were conducted in a furnace operated at a heating rate of 1 °C/min.

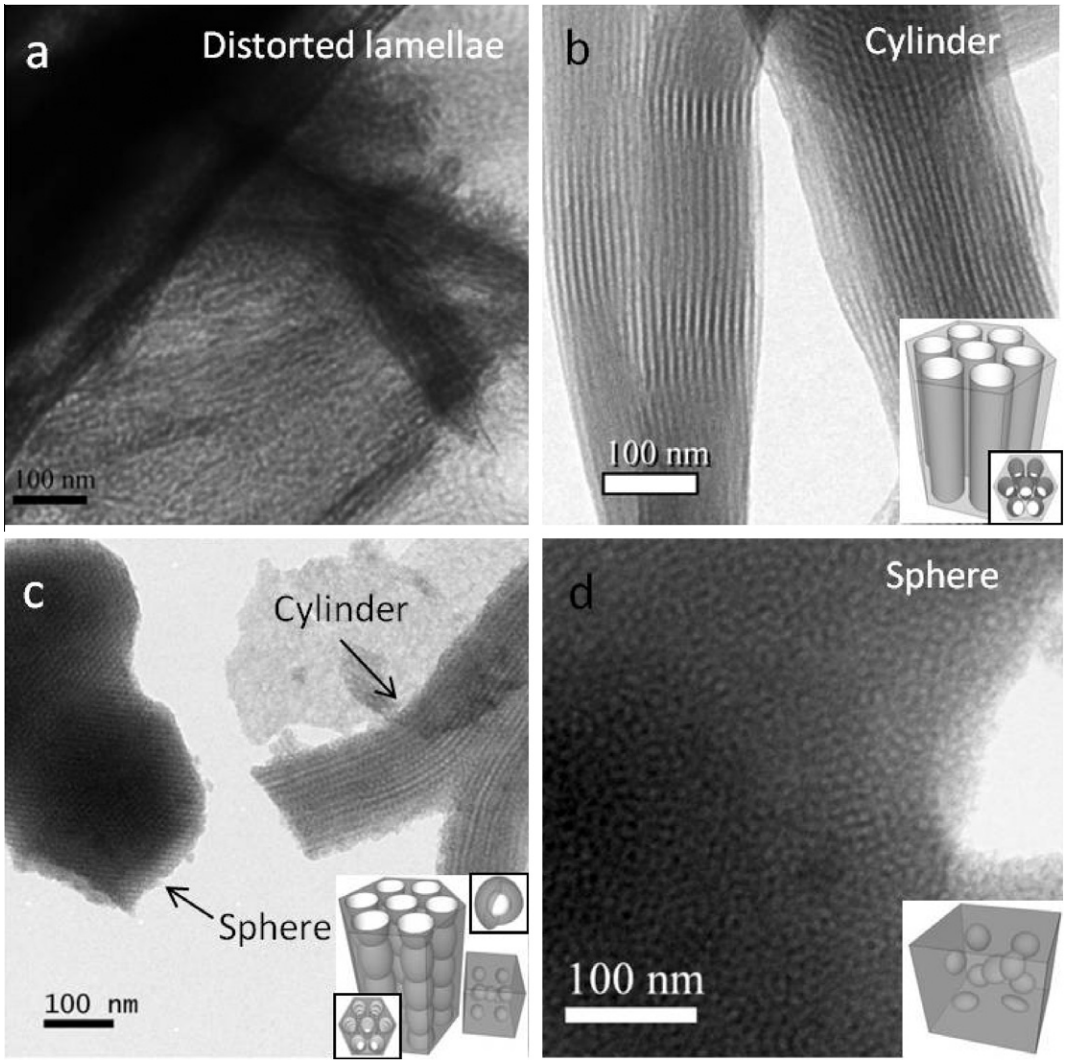

Fig. 2. TEM images of mesoporous silica samples prepared at TEOS-to-PE-*b*-PEO weight ratios of (a) 3.4:1, (b) 5.6:1, (c) 10:1, and (d) 11:1.

2.3. Characterization

SAXS measurements were recorded using a NANOSTAR U small-angle X-ray scattering system (Bruker AXS Gmbh, Karlsruhe, Germany) and Cu Kα radiation (30 W, 50 kV, 600 μA). The *d* spacings were calculated using the formula $d = 2\pi/q$, where *q* is the scattering vector. Transmission electron microscopy (TEM) images were recorded using a JEOL 3010 microscope operated at 200 kV; samples for TEM measurements were suspended in EtOH and supported onto a holey carbon film on a Cu grid. Nitrogen adsorption/desorption isotherms were measured at −196 °C using an ASAP 2020 analyzer; prior to measurements, the samples were degassed under vacuum at 200 °C for at least 6 h. The BET method was used to calculate the specific surface areas and pore volumes; pore size distributions were derived from the adsorption branches of the isotherms by using the Barrett–Joyner–Halenda (BJH) model.

3. Results and discussion

3.1. Mesoporous silica samples synthesized at various TEOS-to-PE-b-PEO ratios

The EISA strategy is used widely because it allows the practical fabrication of various mesoporous nanostructures. Nevertheless, only a few reports have described the processes occurring during EISA. In our present model studies, we used the commercially available block copolymer PE-*b*-PEO as a template and observed

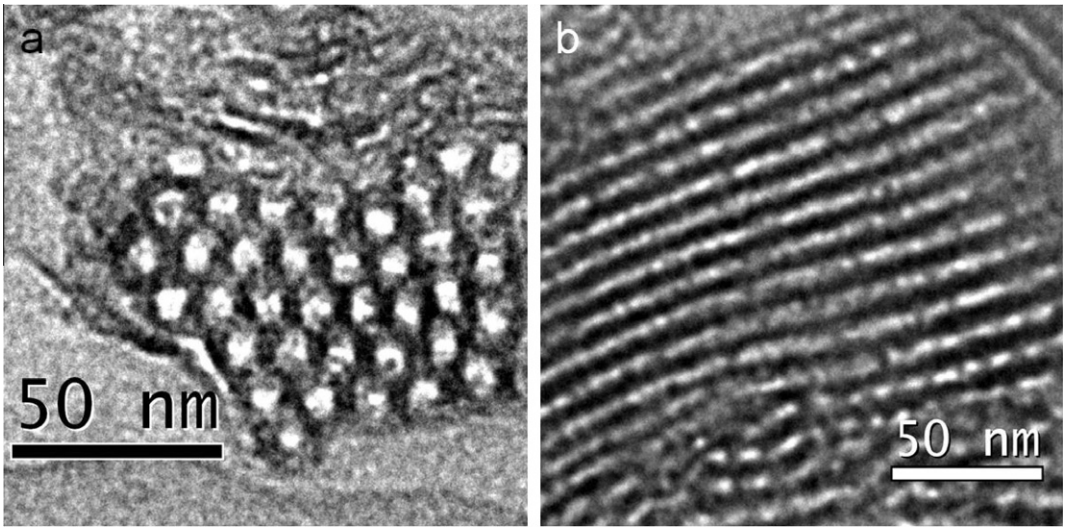

Fig. 3. TEM images of microtomed mesoporous silica samples prepared at a TEOS-to-PE-*b*-PEO weight ratio of 5.6:1. (a) Top view; (b) side view of hexagonal cylinders.

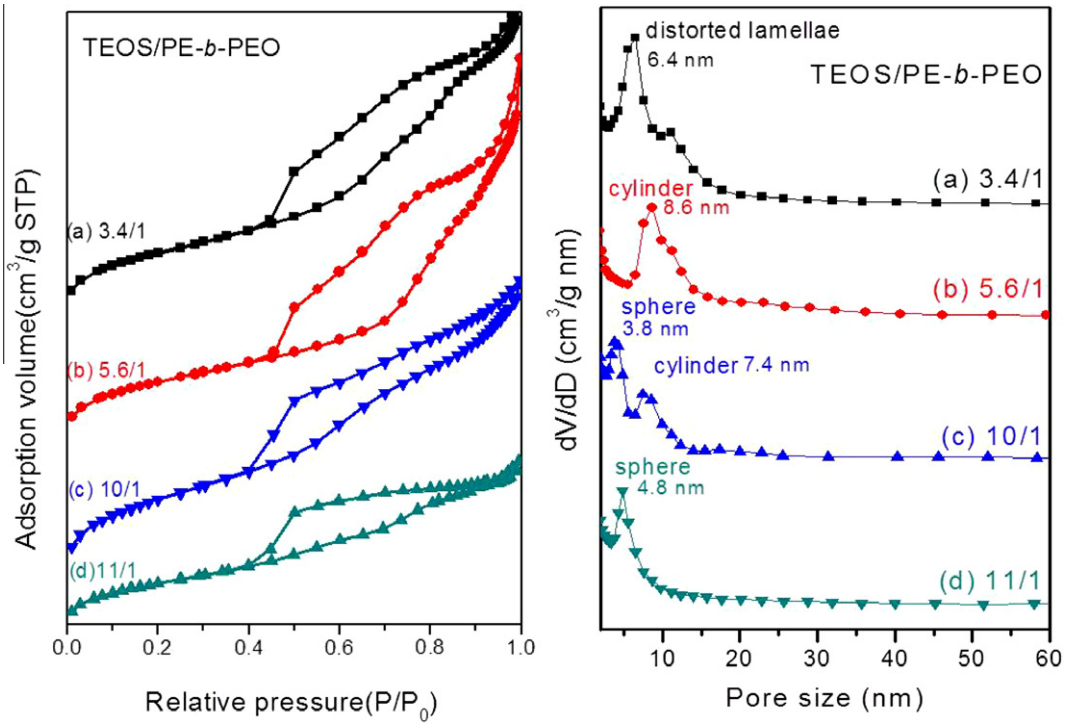

Fig. 4. (A) N_2 adsorption/desorption isotherms and (B) pore size distribution curves of mesoporous silica samples prepared at various TEOS-to-PE-*b*-PEO weight ratios.

the morphological transformations that occurred upon increasing the TEOS-to-PE-*b*-PEO ratio. The mesoporous silica samples featured a distorted lamellar morphology at a relative low TEOS-to-PE-*b*-PEO ratio of 3.4:1, as evidenced by both the SAXS pattern in Fig. 1(a) (only a single peak) and the TEM image in Fig. 2(a). Increasing the TEOS-to-PE-*b*-PEO ratio to 5.6:1 resulted in a cylindrical morphology (Figs. 1(b) and 2(b)). The SAXS pattern in Fig. 1(b) for this sample exhibits its maximum intensity at a value of q^* of approximately 0.571 nm^{-1} (d = 11.0 nm) and higher-order reflections at $3^{1/2}q^*$ and $2q^*$, consistent with a hexagonally packed cylindrical structure. The TEM image in Fig. 2(b) reveals only a side view of the cylindrical structure; the top (Fig. 3(a)) and side (Fig. 3(b)) view TEM images of the microtomed sample provide further evidence for the hexagonal packing of cylindrical structures in the mesoporous silica sample prepared at a TEOS-to-PE-*b*-PEO ratio of 5.6:1. In a previous study, Zhu et al. observed a self-assembled lamellar morphology for a pure PE-*b*-PEO block copolymer [46]. Therefore, we suspect that the cylindrical morphology was transformed from the lamellar structure at lower TEOS-to-PE-*b*-PEO ratios after the EISA process. After increasing the TEOS-to-PE-*b*-PEO ratio to 10:1, SAXS and TEM analyses (Figs. 1(c) and 2(c), respectively) revealed that buckled cylinder and spherical (b.c.c.) structures were coexistent in the material, indicating that the morphology of mesoporous silica sample gradually transformed from hexagonal cylinders to spheres, with the distinctive structure of the buckled cylinders being a metastable phase between the hexagonally packed cylindrical and spherical structures. Zhao et al. reported a similar type of buckled cylindrical structures [45]. Furthermore, the SAXS pattern of this mixed phase revealed two different primary peaks, corresponding to the buckled cylinder and sphere morphologies, respectively. At our highest tested TEOS-to-PE-*b*-PEO weight ratio of 11:1, the SAXS pattern featured only one primary scattering peak, indicating that the morphology of the mesoporous silica sample had returned to only one mesophase (Fig. 1(d)). Fig. 2(d) reveals that the structure of the mesoporous silica sample comprised deformed spheres. Overall, upon increasing the TEOS-to-PE-*b*-PEO ratio, the morphology of the mesophase transformed from lamellae, to distorted lamellae, to hexagonally packed cylinders, to a mixture of buckled cylinders and spheres, and finally to deformed spheres (Scheme 1); therefore, different products were thermodynamically stable at different TEOS-to-PE-*b*-PEO weight ratios at a fixed $HCl_{(aq)}$ content.

The nitrogen sorption isotherms of all of these mesoporous silica samples were representative type-IV curves featuring one or two capillary condensation steps (Fig. 4(A)), suggesting the presence of mesopores with one or two kinds of size. Sample T1 (TEOS/PE-*b*-PEO = 3.4:1) exhibited an H_3-like hysteresis loop at values of P/P_0 ranging from 0.45 to 0.85, indicative of a typical mesoporous structure with slit-like pores (distorted lamellae pores). The H_1-like hysteresis loop of sample T2 (TEOS/PE-*b*-PEO = 5.6:1) was characteristic of cylindrical mesopores. For sample T3 (TEOS/PE-*b*-PEO = 10:1), we observed an interesting phenomenon of two kinds of hysteresis loops, indicating the presence of two types of ordered mesopores; the hysteresis loops at values of P/P_0 ranging from 0.45 to 0.65 (H_2-like loop) and 0.85 to 0.95 (H_1-like loop) are indicative of mesoporous structures featuring spherical and cylindrical pores, respectively. Cubic structures with spherical pores behave H_2 type of hysteresis loop due to the small size interconnections here. Sample T4 (TEOS/PE-*b*-PEO = 11:1) resulted in one H_2-like hysteresis loop, suggesting that it featured spherical pores with only one kind of pore size.

Fig. 4(B) displays the mean pore sizes measured from the adsorption branches, based on the Broekoff-de Boer (BdB) sphere model or the Harkins and Jura model. For sample T1 (distorted lamellae pores), the mean pore size, calculated using the Harkins and Jura model, was 6.4 nm. For sample T2 (cylindrical pores), the mean pore size was 8.6 nm. Two distributions of pore sizes were evident for sample T3, attributable to 3.8-nm spherical pores and 7.4-nm cylindrical pores, respectively. Sample T4 (spherical mesopores) featured only one pore size of 4.8 nm. Table 1 summarizes the d spacings, BET surface areas, pore volumes, and BJH porous sizes of the silica materials.

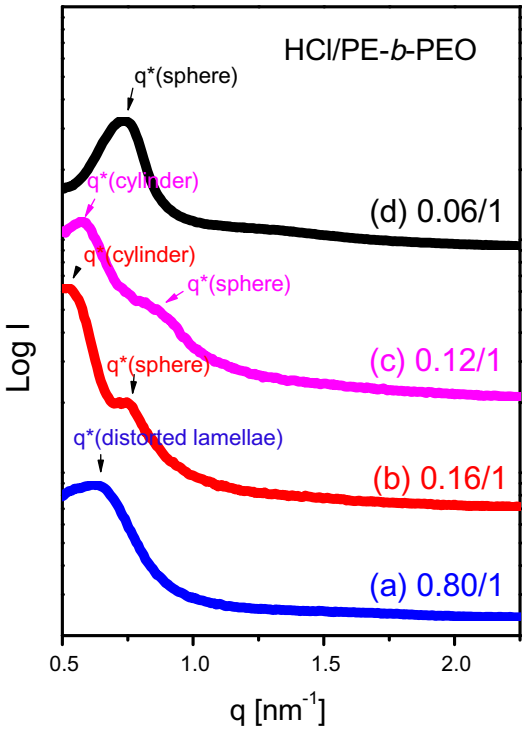

Fig. 5. SAXS patterns of mesoporous silica samples templated by PE-*b*-PEO at various HCl-to-PE-b-PEO weight fractions.

Table 1
Textual properties of the mesoporous silicas.

Sample	d (nm)[a]	Pore size (nm)	S_{BET} (m^2/g)[b]	Pore volume (cm^3/g)	Micropore volume (cm^3/g)	TEOS/PE-*b*-PEO	Morphology
T1	9.1	6.4	493	0.87	0.01	3.4/1	Distorted lamellae
T2	11.0	8.6	475	1.02	0.01	5.6/1	Cylinder
T3	7.2; 9.9	3.8; 7.4	388	0.47	0.02	10/1	Cylinder and sphere
T4	8.7	4.8	639	0.82	0.02	11/1	Sphere
						$HCl_{(aq)}$/PE-*b*-PEO	
H1	9.8	–	131	0.13	0.02	0.80/1	Distorted lamellae
H2	8.3; 11.9	4.8; 7.5	248	0.34	0.02	0.16/1	Cylinder and sphere
H3	7.2; 9.9	3.8; 7.4	388	0.47	0.02	0.12/1	Cylinder and sphere
H4	8.5	4.8	513	0.55	0.02	0.06/1	Sphere

[a] The d-spacing values were calculated by the formula $d = 2\pi/q^*$.
[b] S_{BET} is the total BET surface area calculated from the t-plots.

3.2. Mesoporous silica samples synthesized at different HCl-to-PE-*b*-PEO weight fractions

To study kinetic effects during the EISA fabrication of mesoporous silica samples, we varied the HCl-to-PE-*b*-PEO weight ratio to influence the hydrolysis and condensation rates of TEOS. Fig. 5 displays the SAXS patterns of a series of mesoporous silica samples prepared at different HCl-to-PE-*b*-PEO weight ratios. The SAXS pattern of sample H1 (HCl/PE-*b*-PEO = 0.8:1) reveals a broad scattering peak, implying that its distorted lamellae morphology resulted from the rates of hydrolysis and condensation of TEOS being greater than the rate of self-assembly. The TEM image of sample H1 (Fig. 6(a)) displays its slab-shaped and distorted lamellae structure, consistent with the SAXS pattern. When we decreased the HCl-to-PE-*b*-PEO ratio to 0.16, the SAXS pattern of sample H2 featured two distinct primary peaks that we attribute to cylindrical (d = 9.9 nm) and spherical (d = 7.2 nm) morphologies, respectively. We observed a similar phenomenon for sample H3 (HCl/PE-*b*-PEO = 0.12:1); the ordering of mesoporous silica tended to be improved upon decreasing the amount of acid because the sample has sufficient time to self-assemble during the EISA process. TEM images of the microtomed sample H3 (TEOS/PE-*b*-PEO = 10:1; HCl/PE-*b*-PEO = 0.12:1) revealed two coexisting morphologies: the top-view image in Fig. 7(a) displays cylindrical mesopores and that in Fig. 7(b) features highly ordered mesopores with b.c.c. spherical packing. At a HCl-to-PE-*b*-PEO ratio of 0.06:1, sample H4 exhibited a spherical morphology (Figs. 5(d) and 6(d)). Overall, upon increasing the HCl-to-PE-*b*-PEO weight ratio, the morphology of the mesoporous silica transformed from distorted lamellae, to cylinders mixed with spheres, and finally to spheres. Thus, the morphology tended toward a single regular structure and a thermodynamically stable product when decreasing the amount of acid.

All of the mesoporous silica samples prepared at the different HCl-to-PE-*b*-PEO weight ratios provided typical type-IV isotherms in their N_2 adsorption/desorption curves. Among them, sample H2 displayed two hysteresis loops, but they were difficult to classify; sample H3 also featured two kinds of hysteresis loops, which we attribute to H_2-type (spherical pores, lower P/P_0 range) and H_1-type (cylindrical pores, higher P/P_0 range) samples, respectively. The mesoporous silica of sample H4 provided a single H_2-like hysteresis loop, indicating a rough distribution of spherical mesopores. The pore size distributions of these mesoporous silica samples (Fig. 8(B)) tended toward mono-distribution upon decreasing the amount of $HCl_{(aq)}$; in other words, the morphology tended toward a single thermodynamically stable product upon decreasing the rates of hydrolysis and condensation. On the other hand, the BET surface area (Table 1) increased upon decreasing the amount of $HCl_{(aq)}$, presumably because the rate of silica formation was sufficiently slow to be distributed over the self-assembly system such that there was time for the inorganic species to mix with the

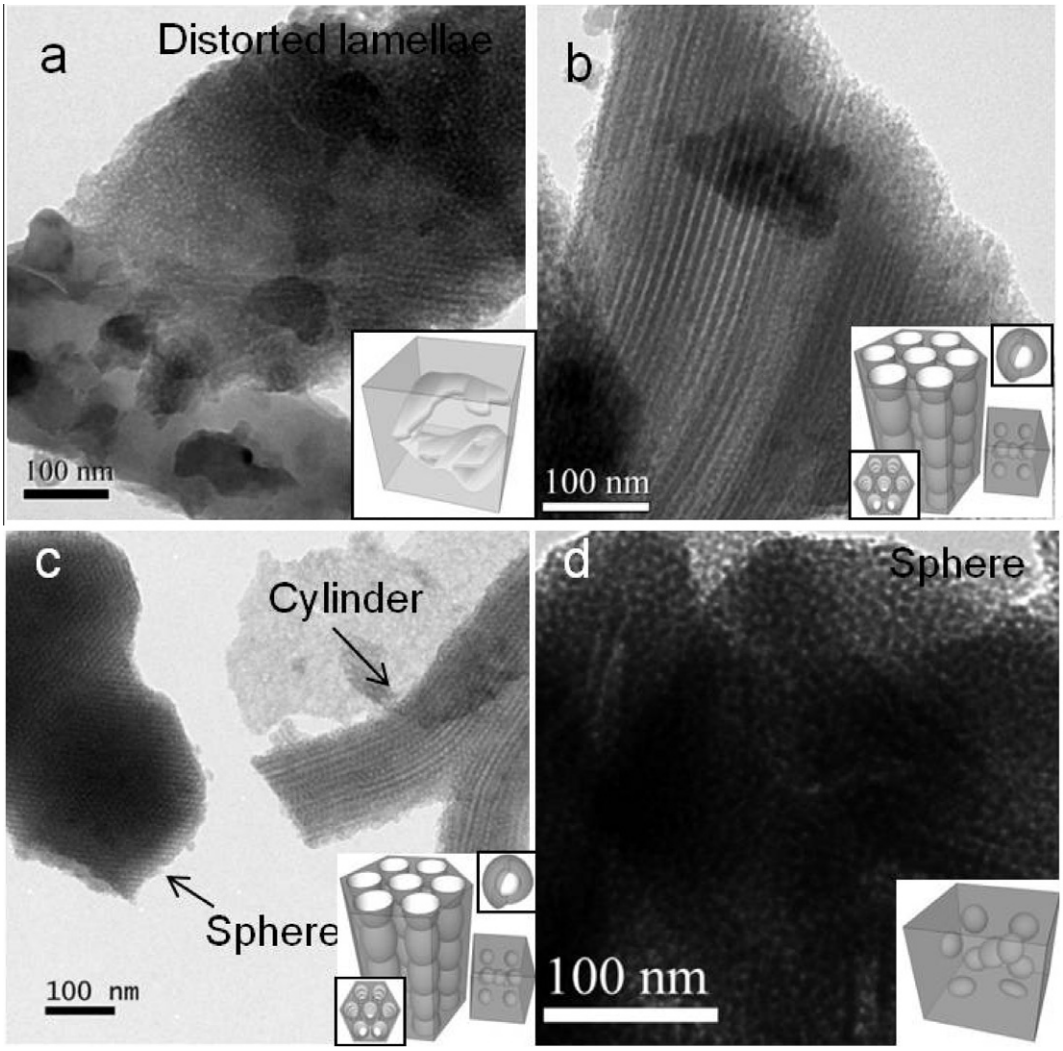

Fig. 6. TEM images of mesoporous silica samples templated by PE-*b*-PEO at HCl-to-PE-*b*-PEO weight ratios of (a) 0.80, (b) 0.16, (c) 0.12, and (d) 0.06.

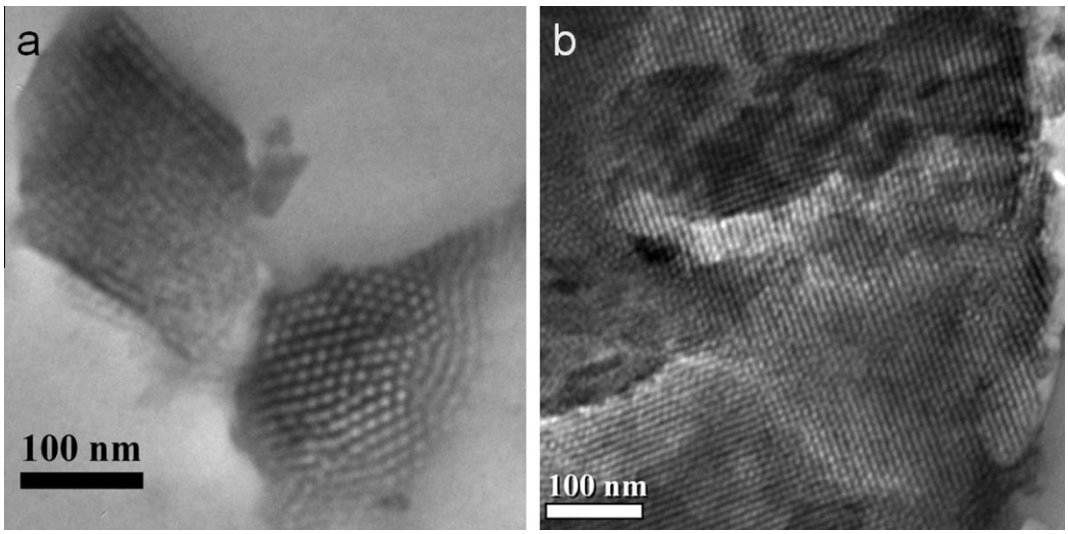

Fig. 7. TEM images of microtomed mesoporous silica samples templated by PE-*b*-PEO at a HCl-to-PE-*b*-PEO weight ratio of 0.12. (a) Hexagonal cylindrical mesopores; (b) spherical mesopores with b.c.c. packing.

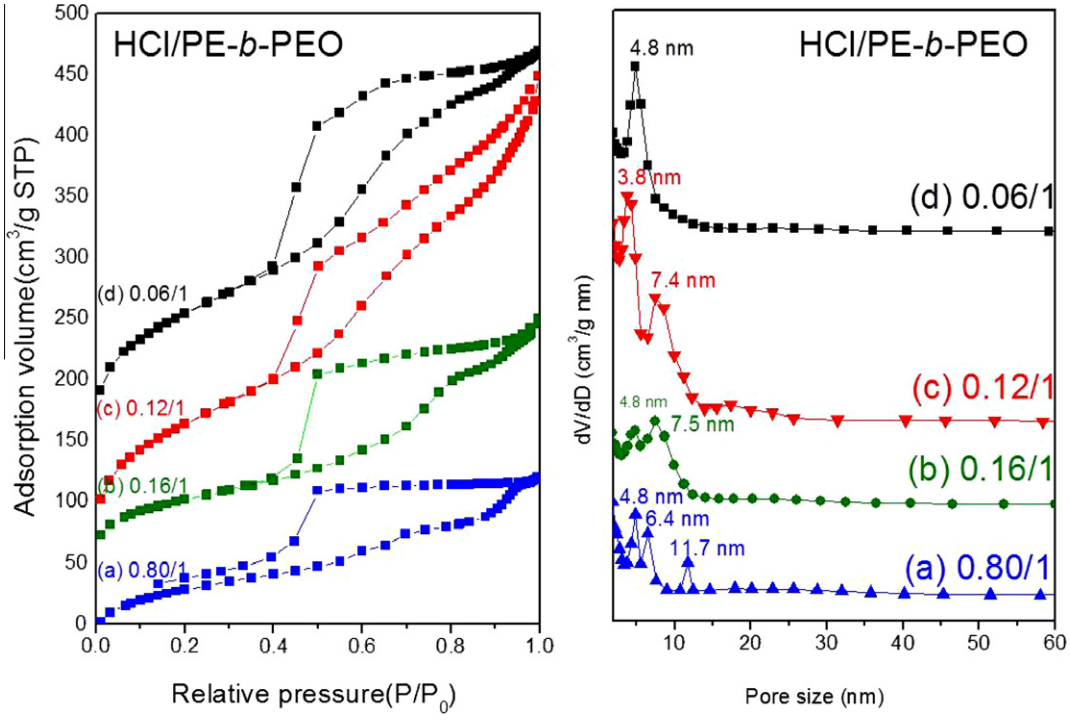

Fig. 8. (A) N_2 adsorption/desorption isotherms and (B) pore size distribution curves of mesoporous silica samples templated by PE-*b*-PEO at various HCl-to-PE-*b*-PEO weight ratios.

organic template during the EISA process. To summarize our findings from varying the TEOS-to-PE-b-PEO and HCl-to-PE-b-PEO ratios, which influenced thermodynamic or kinetic aspects, respectively, the mesophase transformed from lamellae (pure PE-*b*-PEO) to cylinders and spheres upon increasing the TEOS content and from distorted lamellae to cylinders mixed with spheres and finally to disordered spheres upon decreasing the amount of acid.

4. Conclusions

We have used an EISA strategy with PE-*b*-PEO as a template to synthesize ordered mesoporous silica samples having morphologies that could be controlled by changing the amounts of $HCl_{(aq)}$ and TEOS. When we maintained the $HCl_{(aq)}$-to-PE-b-PEO weight ratio steady at 0.12:1 and gradually increased the TEOS-to-PE-*b*-PEO weight ratio, the mesophase transformed from distorted lamellae, to cylinders, to a mixture of buckled cylinders and spheres, and finally to a spherical micelle structure, due to the progressive increase in the volume fraction of the PEO domains. When we fixed the TEOS-to-PE-*b*-PEO ratio at 10:1 and gradually decreased the $HCl_{(aq)}$-to-PE-*b*-PEO weight ratio, the mesophase transformed from distorted lamellae to a mixture of cylinders and spheres and finally to disordered spheres, based on kinetic control. We believe that the formation of each organized hybrid mesostructure resulted from a balance of two competitive processes: (i)

microphase separation and organization of the template and (ii) inorganic polymerization.

Acknowledgment

This study was supported financially by the National Science Council, Taiwan, Republic of China, under contracts NSC 100-2221-E-110-029-MY3 and NSC 100-2628-E-110-001.

References

[1] J.S. Beck, J.C. Vartuli, W.J. Roth, M.E. Leonowicz, C.T. Kresge, K.D. Schmitt, C.T.W. Chu, D.H. Olson, E.W. Sheppard, S.B. McCullen, J.B. Higgins, J.L. Schlenker, J. Am. Chem. Soc. 114 (1992) 10834.
[2] C.T. Kresge, M.E. Leonowicz, W.J. Roth, J.C. Vartuli, J.S. Beck, Nature 359 (1992) 710.
[3] D.Y. Zhao, J.L. Feng, Q.S. Huo, N. Melosh, G.H. Fredrickson, B.F. Chmelka, G.D. Stucky, Science 279 (1998) 548.
[4] D.Y. Zhao, Q.S. Huo, J.L. Feng, B.F. Chmelka, G.D. Stucky, J. Am. Chem. Soc. 120 (1998) 6024.
[5] G. Rother, E.G. Krukowski, D. Wallacher, N. Grimm, R.J. Bodnar, D.R. Cole, J. Phys. Chem. C 116 (2012) 917.
[6] A. Taguchi, F. Schüth, Microporous Mesoporous Mater. 77 (2005) 1.
[7] M. Vallet-Regi, F. Balas, D. Arcos, Angew. Chem. Int. Ed. 46 (2007) 7548.
[8] J. Hu, J.J. Wang, L.H. Zhou, S.H. Xie, H.L. Liu, Acta Phys. Chim. Sin. 22 (2006) 679.
[9] Y.K. Hwang, K.R. Patil, S.H. Jhung, J.S. Chang, Y.J. Ko, S.E. Park, Microporous Mesoporous Mater. 78 (2005) 245.
[10] S.K. Jana, R. Nishida, K. Shindo, T. Kugita, S. Namba, Microporous Mesoporous Mater. 68 (2004) 133.
[11] Q. Xiao, Y.J. Zhong, W.D. Zhu, T.H. Chen, L. Wang, Microporous Mesoporous Mater. 116 (2008) 339.
[12] C.Z. Yu, J. Fan, B.Z. Tian, D.Y. Zhao, Chem. Mater. 16 (2004) 889.
[13] M.C. Chao, C.H. Chang, H.P. Lin, C.Y. Tang, C.Y. Lin, J. Mater. Sci. 44 (2009) 6453.
[14] L. Chen, Y.M. Wang, M.Y. He, J. Porous Mater. 18 (2011) 211.
[15] Q.R. Chen, Y. Sakamoto, O. Terasaki, S.A. Che, Microporous Mesoporous Mater. 105 (2007) 24.
[16] F.Q. Zhang, Y. Meng, D. Gu, Y. Yan, Z.X. Chen, B. Tu, D.Y. Zhao, Chem. Mater. 18 (2006) 5279.
[17] Y. Wan, D.Y. Zhao, Chem. Rev. 107 (2007) 2821.
[18] Y. Wan, Y.F. Shi, D.Y. Zhao, Chem. Commun. (2007) 897.
[19] G. Soler-Illia, E.L. Crepaldi, D. Grosso, C. Sanchez, Curr. Opin. Colloid Interface Sci. 8 (2003) 109.
[20] P.T. Tanev, T.J. Pinnavaia, Science 267 (1995) 865.
[21] S.A. Bagshaw, E. Prouzet, T.J. Pinnavaia, Science 269 (1995) 1242.
[22] G.S. Attard, J.C. Glyde, C.G. Goltner, Nature 378 (1995) 366.
[23] G.S. Attard, P.N. Bartlett, N.R.B. Coleman, J.M. Elliott, J.R. Owen, J.H. Wang, Science 278 (1997) 838.
[24] C.G. Goltner, S. Henke, M.C. Weissenberger, M. Antonietti, Angew. Chem. Int. Ed. 37 (1998) 613.
[25] A.J. Hurd, L. Steinberg, Granular Matter 3 (2001) 19.
[26] C.J. Brinker, MRS Bull. 29 (2004) 631.
[27] C.J. Brinker, Y.F. Lu, A. Sellinger, H.Y. Fan, Adv. Mater. 11 (1999) 579.
[28] D. Grosso, F. Cagnol, G. Soler-Illia, E.L. Crepaldi, H. Amenitsch, A. Brunet-Bruneau, A. Bourgeois, C. Sanchez, Adv. Funct. Mater. 14 (2004) 309.
[29] Q.S. Huo, D.I. Margolese, U. Ciesla, D.G. Demuth, P.Y. Feng, T.E. Gier, P. Sieger, A. Firouzi, B.F. Chmelka, F. Schuth, G.D. Stucky, Chem. Mater. 6 (1994) 1176.
[30] F.S. Bates, G.H. Fredrickson, Phys. Today 52 (1999) 32.
[31] I.W. Hamley, Angew. Chem. Int. Ed. 42 (2003) 1692.
[32] I.W. Hamley, Nanotechnology 14 (2003) R39.
[33] J.G. Li, Y.D. Lin, S.W. Kuo, Macromolecules 44 (2011) 9295.
[34] J. Wei, Y.H. Deng, J.Y. Zhang, Z.K. Sun, B. Tu, D.Y. Zhao, Solid State Sci. 13 (2011) 784.
[35] E. Ortel, T. Reier, P. Strasser, R. Kraehnert, Chem. Mater. 23 (2011) 3201.
[36] Y. Huang, H.Q. Cai, T. Yu, F.Q. Zhang, F. Zhang, Y. Meng, D. Gu, Y. Wan, X.L. Sun, B. Tu, D.Y. Zhao, Angew. Chem. Int. Ed. 46 (2007) 1089.
[37] R.M. Ho, T.C. Wang, C.C. Lin, T.L. Yu, Macromolecules 40 (2007) 2814.
[38] V.R. Tirumala, R.A. Pai, S. Agarwal, J.J. Testa, G. Bhatnagar, A.H. Romang, C. Chandler, B.P. Gorman, R.L. Jones, E.K. Lin, J.J. Watkins, Chem. Mater. 19 (2007) 5868.
[39] Y.H. Deng, T. Yu, Y. Wan, Y.F. Shi, Y. Meng, D. Gu, L.J. Zhang, Y. Huang, C. Liu, X.J. Wu, D.Y. Zhao, J. Am. Chem. Soc. 129 (2007) 1690.
[40] J. Choma, M. Kloske, A. Zawislak, M. Jaroniec, Ochrona Srodowiska 29 (2007) 3.
[41] Y. Deng, C. Liu, D. Gu, T. Yu, B. Tu, D. Zhao, J. Mater. Chem. 18 (2008) 91.
[42] J.G. Li, S.W. Kuo, RSC Adv. 1 (2011) 1822.
[43] J.M. Kim, Y. Sakamoto, Y.K. Hwang, Y.U. Kwon, O. Terasaki, S.E. Park, G.D. Stucky, J. Phys. Chem. B 106 (2002) 2552.
[44] P. Kipkemboi, A. Fogden, V. Alfredsson, K. Flodström, Langmuir 17 (2001) 5398.
[45] C. Liu, Y.H. Deng, J. Liu, H.H. Wu, D.Y. Zhao, Microporous Mesoporous Mater. 116 (2008) 633.
[46] L. Sun, Y.X. Liu, L. Zhu, B.S. Hsiao, C.A. Avila-Orta, Polymer 45 (2004) 8181.